Energy Conversion and Management 65 (2013) 528–538

Contents lists available at SciVerse ScienceDirect

Energy Conversion and Management

journal homepage: www.elsevier.com/locate/enconman

Optimal geometric structure for nanofluid-cooled microchannel heat sink under various constraint conditions

Xiao-Dong Wang *, Bin An, Jin-Liang Xu

State Key Laboratory of Alternate Electrical Power System with Renewable Energy Sources, North China Electric Power University, Beijing 102206, China
Beijing Key Laboratory of Multiphase Flow and Heat Transfer for Low Grade Energy, North China Electric Power University, Beijing 102206, China

ARTICLE INFO

Article history:
Received 19 March 2012
Received in revised form 2 August 2012
Accepted 21 August 2012
Available online 24 October 2012

Keywords:
Nanofluid
Microchannel heat sink
Optimization
Pressure drop
Pumping power
Inlet volume flow rate
Constraint condition

ABSTRACT

A numerical model is developed to analyze the flow and heat transfer in nanofluid-cooled microchannel heat sink (MCHS). In the MCHS model, temperature-dependent thermophysical properties are taken into account due to large temperature differences in the MCHS and strong temperature-dependent characteristics of nanofluids, the model is validated by experimental data with good agreement. The simplified conjugate-gradient method is coupled with MCHS model as optimization tool. Three geometric parameters, including channel number, channel aspect ratio, and width ratio of channel to pitch, are simultaneously optimized at fixed inlet volume flow rate, fixed pumping power, and fixed pressure drop as constraint condition, respectively. The optimal designs of MCHS are obtained for various constraint conditions and the effects of inlet volume flow rate, pumping power, and pressure drop on the optimal geometric parameters are discussed.

1. Introduction

Since the pioneer work by Tuckerman and Pease [1], the MCHS has attracted extensive attention over the past two decades. The MCHS has become an important cooling device to high power light emitting diode, very-large-scale integrated circuits and Micro-Electro Mechanical System applications [1–5]. The performance of a MCHS is closely related to properties of solid material and coolant fluid, to the flow state (laminar flow or turbulent flow, inlet flow rate and temperature of coolant, etc.), and to its geometric structure. The most frequently used coolants in the MCHS study were air, water, and fluorochemicals etc. Recent studies indicated that nanofluids which have high thermal conductivities were applied to MCHS as coolants, the MCHS performance was significantly improved [6–16].

There are two approaches in modeling of nanofluid flow and heat transfer in MCHS. First approach to describe the heat transfer and flow for nanofluid is to treat the nanofluid as a real two-phase mixture in which irregular and random movement of particle increases the heat exchanging rate. The second approach is to treat the nanofluid as a single-phase fluid based on the fact that nanofluid has good uniformity with low particle volume fraction due to nanoscale particle size. In the second approach, the themophysical properties of base fluid, including density, specific heat, thermal conductivity and viscosity, must be substituted by nanofluid's ones. Based on single-phase approach, the thermal conductivity and viscosity of nanofluids have been extensively investigated from both experimental and theoretical viewpoint [17]. The density, thermal conductivity and viscosity of the nanofluids are increased while the specific heat is reduced by the addition of the nanoparticles [18]. The thermal conductivity enhancement mechanisms for nanofluids include the interfacial nanolayer ordering, Brownian motion, Brownian-motion-induced microconvection, particle clustering structures and ballistic transport of energy carriers [18–21].

Table 1 summarizes the recent numerical investigations on nanofluid-cooled MCHS. All models adopted the single-phase approach. Apart from Chen and Ding's model [13], the models were not validated by experiment, because experimental data on flow and heat transfer characteristics for nanofluid-cooled MCHS were available in open literatures until 2007 years [14]. Chein and Chuang [14] tested experimentally the MCHS performance using copper oxide/water nanofluids with 0.2–0.4% particle volume fractions as the coolants. Later, Ho et al. [15] tested experimentally forced convective cooling performance of MCSH with alumina/water nanofluid as the coolant. Both the numerical predictions and the experimental data confirmed that use of nanofluids enhances the cooling performance of MCHS and produces only small increases in pressure drop or pumping power at low particle volume fractions.

* Corresponding author at: State Key Laboratory of Alternate Electrical Power System with Renewable Energy Sources, North China Electric Power University, Beijing 102206, China. Tel./fax: +86 10 62321277.
E-mail address: wangxd99@gmail.com (X.-D. Wang).

0196-8904/$ - see front matter © 2012 Elsevier Ltd. All rights reserved.
http://dx.doi.org/10.1016/j.enconman.2012.08.018

Nomenclature

A_1	convective heat transfer area (m^2)
c_p	specific heat ($J\,kg^{-1}\,K^{-1}$)
D	hydraulic diameter (m)
H_{ch}	channel height (m)
J	objective function
k	thermal conductivity ($W\,m^{-1}\,K^{-1}$)
$k_{nf,eff}$	effective thermal conductivity for the nanofluid flow
L_x	channel length (m)
L_y	height of heat sink (m)
L_z	width of heat sink (m)
N	channel number
p	coolant pressure (Pa)
q_w	heat flux applied to bottom surface of heat sink ($W\,m^{-2}$)
Q	total volumetric flow rate ($m^3\,s^{-1}$)
R_T	total thermal resistance ($K\,W^{-1}$)
T	temperature (K)
u, v, w	velocity component in x, y, z direction ($m\,s^{-1}$)
u_m	average velocity of coolant over channel cross-section ($m\,s^{-1}$)
W_{ch}	channel width (m)
W_r	rib width (m)

Greek

α	aspect ratio of the channel
β	width ratio of channel to pitch
$\gamma_N^{(k)}, \gamma_\alpha^{(k)}, \gamma_\beta^{(k)}$	conjugate gradient coefficients of (N, α, β) in the kth search step
δ	thickness of bottom wall of solid (m)
μ	viscosity ($kg\,m^{-1}\,s^{-1}$)
$\xi_N^{(k)}, \xi_\alpha^{(k)}, \xi_\beta^{(k)}$	search direction of (N, α, β) in the kth search step
ρ	density ($kg\,m^{-3}$)
φ	particle volume fraction
$X_N^{(k)}, X_\alpha^{(k)}, X_\beta^{(k)}$	search step size of (N, α, β) in the kth search step
Ω	pumping power (W)

subscripts

bf	base fluid
in	inlet
l	liquid
nf	nanofluid
out	outlet
p	nanoparticle
s	solid phase

The investigations also found that the geometric structure has remarkable effect on the thermal resistance of nanofluid-cooled MCHS [6,7,10,12]. With different constraint conditions, including fixed pumping power [6,9,10,16], fixed pressure drop [8,10], fixed inlet volume flow rate [13], fixed inlet velocity [7,11], and fixed inlet Reynolds number [12], some conclusions made by these investigations are different. For example, with the fixed pumping power by Tsai and Chein [10] and with the fixed inlet velocity by Li and Kleinstreuer [11] as constraint conditions, the thermal performance of MCHS increases with particle volume fraction, but Ghazvini and Shokouhmand [12] demonstrated that there is an optimal particle volume fraction to reach the maximum heat transfer with fixed inlet Reynolds number. Lelea [16] revealed that contrary to the analysis based on a Re = constant basis, in the fixed pumping power case the heat transfer enhancement rises along the microchannels. Also the heat transfer augmentation increases as the particle's concentration increases. Similarly, the effects on the geometric parameters on the cooling performance are also different in these investigations due to different constraint conditions being used. Tsai and Chein [10] proposed that there are the optimal porosity (ratio of channel width to total width of MCHS) and aspect ratio under a given pressure drop across the MCHS, nanofluids can enhance the MCHS performance when the porosity and aspect ratio are less than the optimum porosity and aspect ratio, oppositely, nanofluids did not produce a significant change in MCHS thermal resistance. Ghazvini and Shokouhmand [12] found that the increase in the porosity and channel aspect ratio always improved MCHS performance under fixed inlet Reynolds number.

The fixed pumping power condition for evaluating cooling performance of the MCHS is physically practical constraint condition because which means the power required to drive the fluid through the MCHS is the same. However, from the viewpoint of practical operation of MCHS the fixed inlet volume flow rate or pressure drop is more easily controlled. In addition, for a MCHS, the geometric parameters include the channel number, the channel aspect ratio, and the width ratio of channel to pitch, and all parameters have coupled effect on the MCHS cooling performance. An individual parameter study is useful but it cannot answer how one can obtain the optimal design. Therefore, a multi-parameter coupled/combined effect is needed to account for to obtain optimal nanofluid-cooled MCHS performance. Based on the above reasons, this work develops an inverse problem optimization method, which combines a complete three-dimensional solid–fluid conjugated MCHS model and simplified conjugate-gradient method, to optimize geometric parameters of nanofluid-cooled MCHS for various constraint conditions, including fixed inlet volume flow rate, the fixed pumping power, and fixed pressure drop. In the MCHS model, temperature-dependent thermophysical properties are taken into account due to large temperature differences in the MCHS and strong temperature-dependent characteristics of nanofluids, the model is validated by experimental data by Ho et al. [15] with good agreement. The optimal designs of MCHS are obtained for various constraint conditions and the effects of pumping power, inlet volume flow rate, and pressure drop on the optimal geometric parameters are discussed.

2. Parameters of nanofluid-cooled MCHS for optimization

The schematic of MCHS with dimensions of $L_x = 10$ mm, $L_y \leqslant 1$ mm, and $L_z = 10$ mm is shown in Fig. 1, which consists of N parallel microchannels and N ribs with rectangular cross-section. Usually, the bottom of the MCHS is mounted on electronic equipment or other heat dissipating component. Heat is removed primarily by conduction through the solid and then dissipated away by convection of the cooling fluid in the microchannels. The channel has a height H_{ch}, width W_{ch}, and the rib has a width W_r with the same height as the channel, thus, we have $W_{ch} + W_r = L_z/N$. The thickness of the top and bottom plates are fixed to $\delta = 0.1$ mm. The channel aspect ratio and the width ratio of channel to pitch are defined as $\alpha = H_{ch}/W_{ch}$, $\beta = W_{ch}/(W_{ch} + W_r)$, respectively. Once N, α, and β are given, the geometric structure of the MCHS is determined uniquely. Therefore, N, α, and β are chosen as optimized parameters and are optimized simultaneously at fixed inlet volume flow rate, fixed pumping power, and fixed pressure drop in the present work, respectively.

3. Optimization method

3.1. The nanofluid-cooled MCHS model

The solid–fluid conjugated model is refined from that adopted in our previous work for water-cooled MCHS [5] with modified

Table 1
A review of previous numerical study on nanofluid-cooled MCHS.

Researchers (Year)	Model	Constraint conditions	Nanofluid	Model validation	Content	Conclusions
Chein and Huang [6]	Single-phase method, analytical model with experimental correlations	Fixed pumping power	Cu/H_2O	No	The thermal resistances and pressure drops of MCHS using nanofluids with various particle volume fractions for two specific geometries were discussed	Performances were greatly improved and no extra pressure drop is produced when nanofluids were used as the coolants. Channel geometry has significant effect on the MCHS performance
Koo and Kleinstreuer [7]	Single-phase, solid–fluid conjugated model	Fixed inlet flow velocity	CuO/H_2O, $CuO/C_2H_6O_2$	No	The effects of nanoparticle volume fractions on the microchannel pressure drops, temperature profiles and Nusselt numbers are computed and analyzed	A base fluid of high-Prandtl number, nanoparticles of high thermal conductivity, and a channel with high aspect ratio is recommended
Abbassi and Aghanajafi [8]	Single-phase, porous media model	Fixed pressure drop	Cu/H_2O	No	The effects of nanoparticle volume fractions, thermal dispersion coefficient and Reynolds number on thermal performance of MCHS were investigated	Using nanofluid leads to astonishing heat transfer enhancement in MCHS and this enhancement increases with increasing flow Reynolds number and particle volume fraction
Jiang and Choi [9]	Single-phase, solid–fluid conjugated model	Fixed pumping power	Cu/H_2O, DIA/H_2O	No	Thermal resistances of MCHS with water and water-based nanofluids were compared	The cooling performance of a MCHS with 1% volume fraction water-based nanofluids at the fixed pumping power of 2.25 W is enhanced by about 10% compared with that of a MCHS with water
Tsai and Chein [10]	Single-phase, porous media model	Fixed pumping power or fixed pressure drop	Cu/H_2O, CNT/H_2O	No	Thermal resistances of MCHS with nanofluids for various porosities and channel aspect ratios were compared	Under a given pressure drop across the MCHS, nanofluid can enhance the MCHS performance when the porosity and aspect ratio are less than the optimum porosity and aspect ratio. When the porosity and channel aspect ratio are higher than optimum porosity and aspect ratio, the nanofluid did not produce a significant change in MCHS thermal resistance
Li and Kleinstreuer [11]	Single-phase, solid–fluid conjugated model	Fixed inlet flow velocity	CuO/H_2O	No	Thermal resistances and pressure drops of MCHS using nanofluids with various particle volume fractions were investigated	Nanofluids measurably enhance the thermal performance of microchannel mixture flow with a small increase in pumping power. Specifically, the thermal performance increases with volume fraction; but, the extra pressure drop, or pumping power, will somewhat decrease the beneficial effects
Ghazvini and Shokouhmand [12]	Single-phase, fin model and porous media model	Fixed inlet Reynolds number	Inlet CuO/H_2O	No	The effects of particle volume fraction, porosity, channel aspect ratio and on the heat transfer of MCHS were compared using Fin model and porous media model	The porous media model is better to predict MCHS performance than the Fin model. There is an optimal particle volume fraction to reach maximum heat transfer. Increase in channel aspect ratio and porosity improved MCHS performance
Chen and Ding [13]	Single-phase, porous media model	Fixed inlet volume flow rates	Al_2O_3/H_2O	Yes	The Forchheimer Brinkman extended Darcy equationis with an inertial force term were used to describe the fluid flow. Thermal resistances of MCHS using nanofluids with various particle volume fractions are compared	The temperature distributions of the channel wall is practically not sensitive to the inertial effect, while the fluid temperature distribution and the total thermal resistance change significantly due to the inertial force effect, thus; the thermal resistance is overestimated as the inertial effect is neglected

Notes: CNT denotes the carbon nanotube, DIA denotes the diamond.

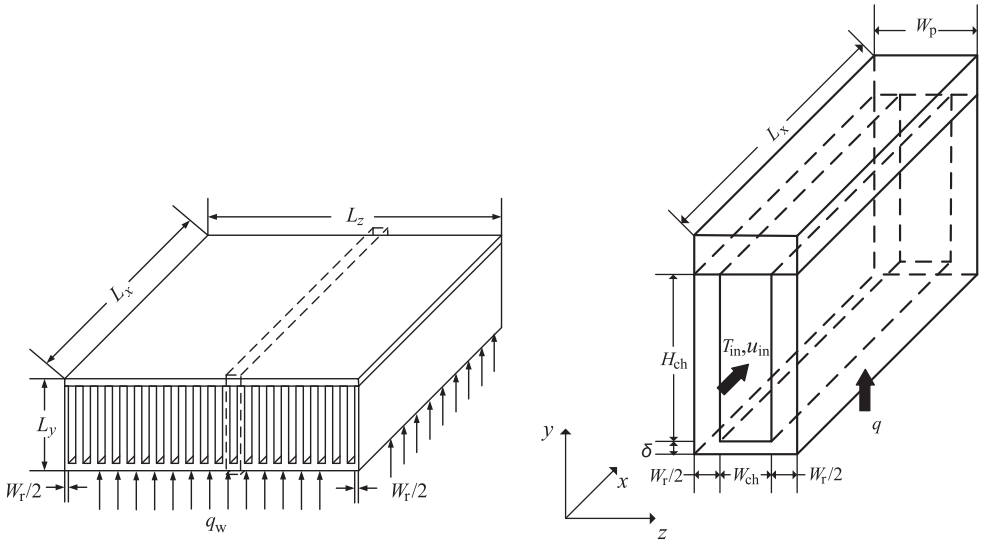

Fig. 1. Schematics of MCHS and computational region.

nanofluid thermophyical properties. The model assumes that the system is steady; the flow is laminar; the effects of gravitational force, radiation heat transfer, and contact resistance at the interfaces between solid wall and coolant are neglected. The model includes continuity, momentum and energy equations for fluid region and energy equation for solid region. The main governing equations and corresponding boundary conditions are listed in Appendix A.

For all constraint conditions, the inlet velocity must be given to numerically solve Eqs. (A1)–(A7). Under fixed pumping power condition, the inlet velocity of the nanofluid, u_{in}, is calculated as follows [5]:

$$u_{in} = \left(\frac{4\alpha}{2\mu_{nf}(4.70(1+\alpha)^2 + 19.64(1+\alpha^2))} \frac{\Omega}{NL_x} \right)^{0.5} \tag{1}$$

where Ω is the pumping power.

Under fixed inlet volume flow rate, the inlet velocity can be calculated as follows:

$$u_{in} = \frac{Q_V}{NH_{ch}W_{ch}} \tag{2}$$

where Q_V is the inlet volume flow rate.

Under fixed pressure drop, the inlet velocity can be calculated as follows:

$$u_{in} = \frac{D^2(1+\alpha)^2\Delta p}{2\mu_{nf}L_x(4.70(1+\alpha)^2 + 19.64(1+\alpha^2))} \tag{3}$$

where $D = 2H_{ch}W_{ch}/(H_{ch} + W_{ch}) = 2\alpha\beta L_z/(N(1+\alpha))$ is the hydraulic diameter, Δp is the pressure drop.

The water-based Al_2O_3 nanofluid with 1% particle volume fraction is used as the coolant of MCHS. The assumption of constant thermophyiscal properties for nanofluids were adopted in the previous investigations [6,8–10,12,13], Li and Kleinstreuer [11] proposed that the thermal conductivity and viscosity of nanofluids have strong temperature-dependent characteristics and large temperature difference may occurs in the MCHS, especially under high heat removal conditions. Therefore, the temperature-dependent properties are adopted in the present model.

The nanofluid density, ρ_{nf}, and thermal capability, $(\rho c_p)_{nf}$, are calculated using mixing theory [22]:

$$\rho_{nf} = \varphi\rho_p + (1-\varphi)\rho_{bf} \tag{4}$$

$$(\rho c_p)_{nf} = \varphi(\rho c_p)_p + (1-\varphi)(\rho c_p))_{bf} \tag{5}$$

where ρ_{nf}, ρ_{bf} and ρ_p are the densities of nanofluid, base liquid and nanoparticle, respectively, φ is the volume fraction of nanoparticle, $c_{p,nf}$, $c_{p,bf}$ and $c_{p,p}$ are the specific heats of nanofluid, base fluid and nanoparticle, respectively. Different from previous investigations [6,8–10,12,13], the present work correlates the density and specific heat for base liquid (water) as polynomial functions of temperature [23].

The experimental data for the thermal conductivity and viscosity of $\varphi = 1\%$ Al_2O_3 nanofluid are used to obtain temperature-dependent correlations. The viscosity correlation is fitted using experimental data by Nguyen et al. [24] and can be expressed as:

$$\mu_{nf} = c_0 + c_1T + c_2T^2 + c_3T^3 \tag{6}$$

where μ_{nf} is the nanofluid viscosity, $c_0 = 187.1725 \times 10^{-3}$, $c_1 = -1.6551 \times 10^{-3}$, $c_2 = 4.9134 \times 10^{-6}$, $c_3 = -4.8839 \times 10^{-9}$. Comparison of experimental viscosity data with Eq. (6) shows sufficient agreement with maximum deviation of 3.8%. The thermal conductivity correlation is fitted using experimental data by Das et al. [25] expressed as:

$$k_{nf} = c_0 + c_1T \tag{7}$$

where k_{nf} is the thermal conductivity of nanofluid, $c_0 = -0.3687$ and $c_1 = 3.3497 \times 10^{-3}$ are fitted parameters, and T is absolute temperature. Eq. (7) has good agreement with experimental data (maximum deviation of 0.7%).

For the nanofluid, effective thermal conductivity in a flowing system is larger than that at stationary state due to the thermal dispersion effect caused by random motion of nanoparticles. Experimental thermal conductivity by Das et al. [25] was tested at stationary state and hence Eq. (7) does not consider the thermal dispersion contributed to the heat transfer. With this consideration, Xuan and Roetzel [26] proposed a modified effective thermal conductivity of nanofluid for forced convection heat transfer as follows:

$$K_{nf,eff} = k_{nf} + C^*(\rho c_p)_{nf}\varphi(H_{ch}/2)u_m \tag{8}$$

where $k_{nf,eff}$ is the effective thermal conductivity for the nanofluid flow, u_m is the average velocity in the channel equal to the inlet velocity u_{in}, and C^* is an experimentally determined parameter. We used nanofluid-cooled MCHS model (Eqs. (A1)–(A9)) with modified thermophysical properties Eqs. (4)–(8) to predict the MCHS

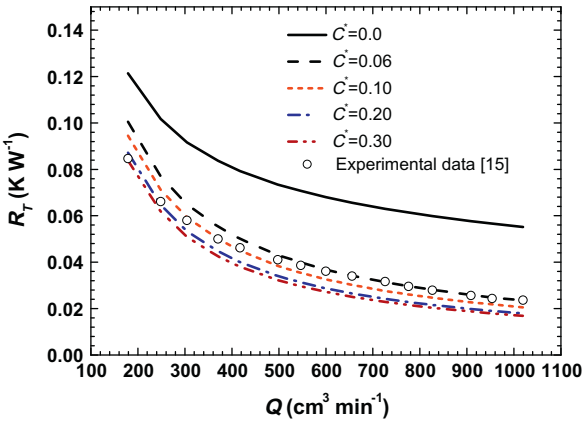

Fig. 2. Total thermal resistances for water-based Al_2O_3 nanofluid with 1% particle volume fraction predicted by the present model with various C^*.

performance. Comparison of predicted and experimental thermal resistances [15] for $\varphi = 1\%$ Al_2O_3 nanofluid under the same MCHS geometry and operation conditions indicates that C^* is dependent on nanofluid volume flow rates (Fig. 2). The best fitted C^* are applied: $C^* = 0.30$ for $Q_V < 200\ cm^3\ min^{-1}$; $C^* = 0.20$ for $200\ cm^3\ min^{-1} \leqslant Q_V < 300\ cm^3\ min^{-1}$; $C^* = 0.10$ for $300\ cm^3\ min^{-1} \leqslant Q_V < 500\ cm^3\ min^{-1}$; $C^* = 0.06$ for $Q_V \geqslant 500\ cm^3\ min^{-1}$. The curve with $C^* = 0$ corresponds to no thermal dispersion effect, which yields a much higher thermal resistance than experimental data. Hence, thermal dispersion effect enhances heat transfer rate for the present nanofluid force convection system.

3.2. Simplified conjugate-gradient method

The main equations of simplified conjugate-gradient method are listed in Appendix B. The objective function to be optimized can be expressed as follows:

$$J = F(N, \alpha, \beta) \tag{9}$$

where the parameters for optimization N, α, and β are referred to as search variable. In the present study, the objective function, J, is defined as the total thermal resistance expressed as:

$$R_T = \frac{T_{max} - T_{min}}{q_w A} = \frac{T_{max} - T_{in}}{q_w A} \tag{10}$$

where T_{max} and T_{min} are the maximum and minimum temperatures observed in the heat sink. T_{min} is equal to the inlet temperature of the coolant, T_{in}. Therefore, an optimal set of geometric parameters N, α, and β is searched for to reach the minimum of the objective function.

In the simplified conjugate-gradient method [27], the values of the step size β_i are claimed to fix at a constant value without loss of convergence. That is,

$$\beta_i = C_i \quad i = 1, 2, 3 \tag{11}$$

The magnitude of C_i can be different for each search variable in accordance with its sensitivity to the objective function. Note that the convergence speed of the iteration of the optimization process may be slightly slowed down by a fixed step size; however, the need to determine the one-dimensional search of step size for each β_i has been removed.

3.3. Optimization scheme

The initial guess for each search variable is made first, and in the successive steps the conjugate-gradient coefficients and the search directions are evaluated to estimate the new search variables. This process is repeated to reach the minimum of the objective function. Specifically, the procedures are listed as follows:

(1) Make the initial guess for the search variables N, α, and β, assign the values to the step sizes β_1–β_3.
(2) Create geometry and grids of MCHS model for the assigned N, α, and β. Specify all boundary conditions, and then numerically solve Eqs. (A1)–(A9).
(3) Calculate the objective function $J(N, \alpha, \beta)$ based on Eq. (10). If the convergence criterion is satisfied, then terminate iteration; otherwise, proceed to step (4).
(4) Calculate the sensitivity coefficients $\partial J/\partial N$, $\partial J/\partial \alpha$, and $\partial J/\partial \beta$ of the objective function for each search variable based on Eq. (A10).
(5) Calculate the conjugate-gradient coefficients $\gamma_i^{(k)}$ for the each search variable based on Eq. (A13). For the first step with $k = 1$, $\gamma_i^{(1)} = 0$ ($i = 1, 2, 3$).
(6) Calculate the search directions, $\xi_i^{(k)}$, for the each search variable based on Eq. (A12).
(7) Update new search variables based on Eq. (A11) and then return to step (2).

In steps (2) and (4), the MCHS model, Eqs. (A1)–(A9), were converted to the finite-difference form by the control volume method and were solved iteratively with an iteration criterion for convergence of 10^{-6}. It is noticeable that the parameter N as a search variable must be an integer in every search step. The nanofluid-cooled MCHS model and simplified conjugate-gradient model are coupled and solved using self-built Fortran program.

4. Individual parameter study

In the individual parameter study, the heat sink has $L_x = 10$ mm, $L_z = 10$ mm, and L_y is allowed to exceed 1 mm to obtain a large α. The thickness of the bottom wall, pumping power and q_w are fixed at 100 μm, 0.05 W, and 100 W cm^{-2}, respectively. The water-based Al_2O_3 nanofluid with 1% particle volume fraction is used as the coolant of MCHS, and its inlet temperature is assumed to be 293 K. The constraint conditions are as follows: fixed inlet volume flow rate $Q_V = 200\ cm^3\ min^{-1}$, fixed pumping power $\Omega = 0.05$ W, and fixed pressure drop $\Delta p = 20$ kPa, respectively.

For optimization with fixed pressure drop as the constraint condition, the outlet pressure is assumed to be 1.01325×10^2 kPa, and inlet pressure drop is assumed to be $1.01325 \times 10^2 + 20$ kPa, the inlet flow velocity is unknown and is needed to solve. However, in order to calculate the effective thermal conductivity of nanofluid (Eq. (8)), the inlet flow velocity of nanofluid must be given before numerical simulation. Therefore, Eq. (3) is adopted to calculate the inlet flow velocity using known pressure drop. Fig. 6 compares the difference of the inlet flow velocities between calculated by Eq. (3) and predicted by numerical simulation by use of fixed pressure inlet as boundary condition. It can be seen that both velocities agree well for various nanofluid-cooled MCHS geometries during whole optimization process.

4.1. Fixed inlet volume flow rate

Effects of the channel number, channel aspect ratio, and width ratio of channel to pitch on the total thermal resistance of nanofluid-cooled MCHS when the volume flow rate was fixed at $Q_V = 200\ cm^3\ min^{-1}$ are shown in Fig. 3.

Fig. 3a shows that under fixed Q_V, increasing the channel number, N, reduces the total thermal resistance. This can be explained as follows. The inlet flow velocity of nanofluid meets

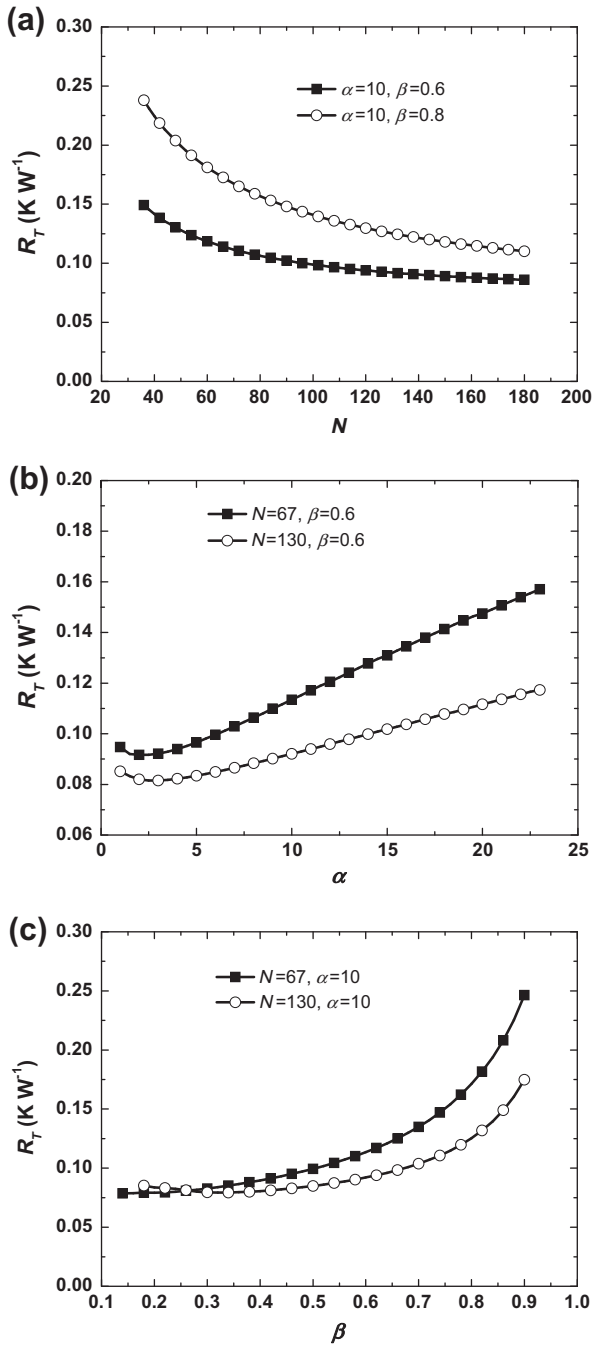

Fig. 3. Total thermal resistances for various MCHS geometries at fixed volume flow rate of 200 cm^3 min^{-1}: (a) channel number; (b) channel aspect ratio; and (c) width ratio of channel to pitch.

$u_{in} = Q_V/(\alpha\beta L_z W_{ch}) = Q_V/(\beta L_z H_{ch})$, as N increases W_{ch} and H_{ch} decrease under fixed α and β, which elevates u_{in} and enhances convective heat transfer of nanofluid, meanwhile, according to Eq. (8) increase in N does not change the effective thermal conductivity of nanofluid, thus, higher N reduces the total thermal resistance. It also can be seen from Fig. 3a that at the same channel number, heat sink with $\alpha = 10$, $\beta = 0.6$ has smaller thermal resistance than with $\alpha = 10$, $\beta = 0.8$, because small β increases the flow velocity and convective heat transfer. At large N, the flow velocity is enough high, hence the reduction rate in the thermal resistance for a large N is less than that for a small N.

Fig. 3b shows that with $N = 67$ and $\beta = 0.6$, the thermal resistance first decreases and then increases with an optimal value $\alpha = 3.5$. The same tendency occurs for $N = 130$ and $\beta = 0.6$, giving the same optimal value $\alpha = 3.5$. With fixed N and β, increasing α increases channel height $H_{ch} = \alpha W_{ch} = \alpha\beta L_z/N$, which reduces the inlet flow velocity and increases the convective heat transfer area $A_1 = 2N(W_{ch} + H_{ch})L_x = 2(1 + \alpha)\beta L_z L_x$. Thus, the total convective heat transfer between nanofluid and channel wall depends on competition of u_{in} and A_1, hence there is an optimal α.

Fig. 3c shows that the total thermal resistance increases monotonously with β. With fixed N and α, increasing β increases both the channel width $W_{ch} = \beta L_z/N$ and the channel height $H_{ch} = \alpha W_{ch}$, thus reduces $u_{in} = Q_V/(\alpha\beta L_z W_{ch})$ and increases $A_1 = 2(1 + \alpha)\beta L_z L_x$. In addition, according to Eq. (8), $k_{nf,eff} = k_{nf} + 0.5C^*(\rho c_p)\varphi H_{ch} u_{in} = k_{nf} + 0.5$-$_{nf,eff} = k_{nf} + 0.5C^*(\rho c_p)\varphi H_{ch} u_{in} = k_{nf} + 0.5C^*(\rho c_p)\varphi QV/(\beta L_z)$, increas-

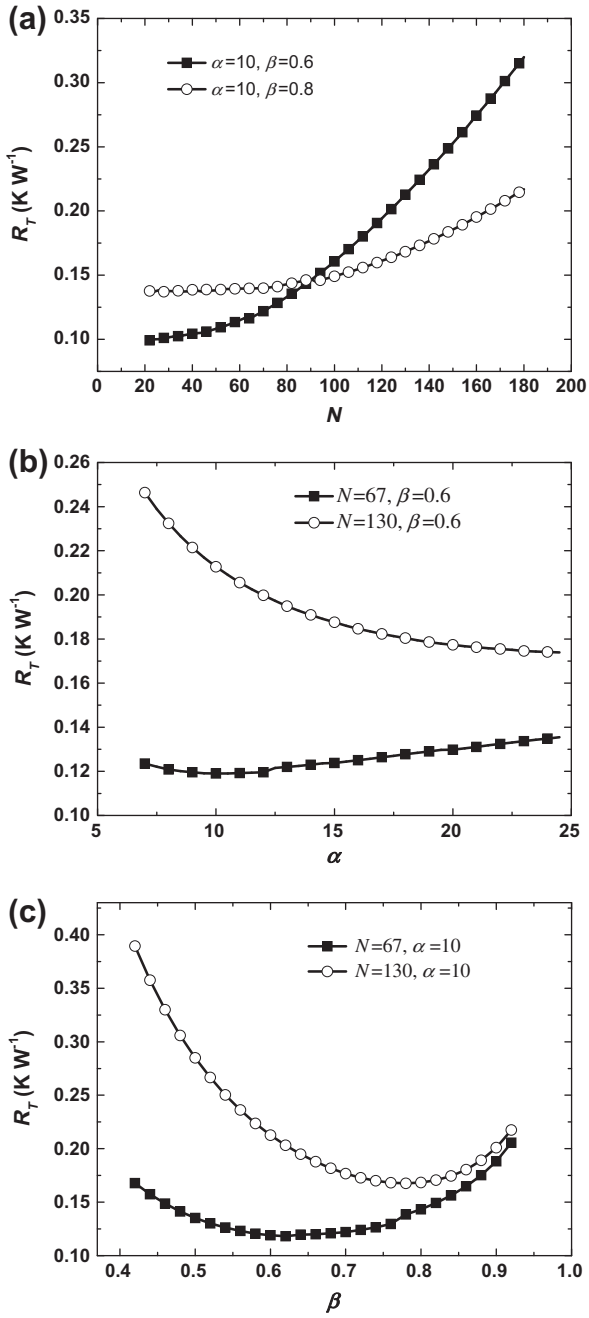

Fig. 4. Total thermal resistances for various MCHS geometries at fixed pumping power of 0.05 W: (a) channel number; (b) channel aspect ratio; and (c) width ratio of channel to pitch.

ing β also reduces the effective thermal conductivity of nanofluid. Therefore, small β is better to enhance nanofluid-cooled MCHS heat transfer.

4.2. Fixed pumping power

Fig. 4 shows the effect of channel number, channel aspect ratio, and width ratio of channel to pitch on the total thermal resistance when the pumping power was fixed at 0.05 W. As N increases, the total thermal resistance increases (Fig. 4a). The MCHS with $\alpha = 10$, $\beta = 0.6$ has lower thermal resistance than that with $\alpha = 10$, $\beta = 0.8$ for $N < 92$, however, it has higher thermal resistance for $N > 92$. It is can be seen from Eq. (1) that under fixed pumping power and with fixed α and β, increasing N reduces the inlet flow velocity and hence reduces the convective heat transfer. In addition, increasing N also decreases H_{ch}, which causes a reduction in the effective thermal conductivity of nanofluid. Thus, large N significantly deteriorates the cooling performance of nanofluid-cooled MCHS.

Fig. 4b shows that as α increases, the thermal resistance decreases for heat sink with $N = 130$ and $\beta = 0.6$, however, the thermal resistance first decreases and then increases with an optimal value $\alpha = 10$ for heat sink with $N = 67$ and $\beta = 0.6$. With fixed N and β, increasing α reduces u_{in} according to Eq. (1), however, it also increases the convective heat transfer area $A_1 = 2(1+\alpha)\beta L_z L_x$ and the effective thermal conductivity $k_{nf,eff} = k_{nf} + 0.5C^*(\rho c_p)\varphi H_{ch}$-$_{nf,eff} = k_{nf} + 0.5C^*(\rho c_p)\varphi H_{ch}u_{in} = k_{nf} + 0.5C^*(\rho c_p)\varphi u_{in}\alpha\beta L_z/N$, so that there is an optimal value of α. Large $N = 130$ has small u_{in}, which causes that as α increases, the increase in A_1 and $k_{nf,eff}$ for $N = 130$ is less than for $N = 63$. Therefore, the optimal value still does not occur up to $\alpha = 24.5$ for $N = 130$.

Fig. 4c shows that with fixed N and α, there is an optimal β. The optimal value is $\beta = 0.62$ for $N = 67$ and $\alpha = 10$, and $\beta = 0.78$ for $N = 130$ and $\alpha = 10$. With fixed N and α, increasing β does not change u_{in} according to Eq. (1), but increases the convective heat transfer area $A_1 = 2(1+\alpha)\beta L_z L_x$ and the effective thermal conductivity of nanofluid $k_{nf,eff}$. Thus, larger β enhances convective heat transfer of nanofluid. However, large β also reduces the rib width W_r, which increases the conductive thermal resistance through the solid silicon; hence too large β is not recommended.

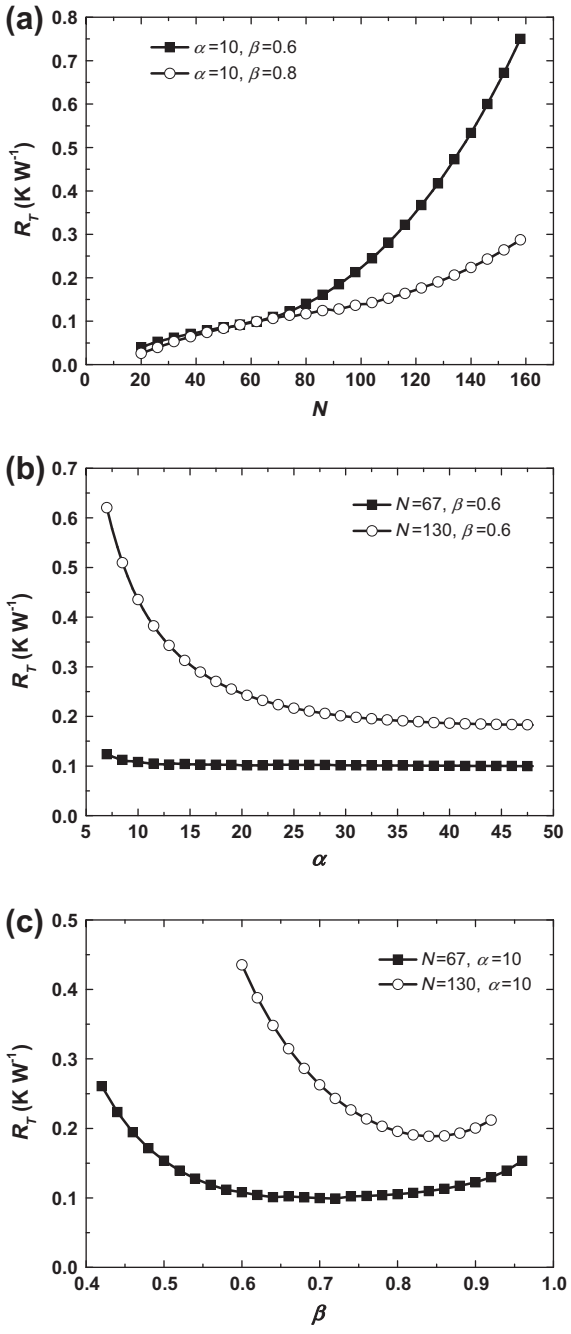

Fig. 5. Total thermal resistances for various MCHS geometries at fixed pressure drop of 20 kPa: (a) channel number; (b) channel aspect ratio; and (c) width ratio of channel to pitch.

4.3. Fixed pressure drop

Fig. 5 shows the effect of channel number, channel aspect ratio, and width ratio of channel to pitch on the total thermal resistance under the constant pressure drop $\Delta p = 20$ kPa as constraint condition. When the pressure drop is fixed at 20 kPa, with constant α and β, increasing N reduces u_{in} because u_{in} is proportional to N^{-2} according to Eq. (3). Increasing N also reduces H_{ch} and results in a reduced $k_{nf,eff}$ according to Eq. (8). Thus, large N decreases convective heat transfer of nanofluid and hence reduces the total thermal resistance (Fig. 5a).

Fig. 5b shows that increasing α decreases the total thermal resistance under fixed N and β because increasing α increases both u_{in} and $k_{nf,eff}$. Since high N decreases convective heat transfer the thermal resistance of heat sink with $N = 67$ and $\beta = 0.6$ is far less than that with $N = 130$ and $\beta = 0.6$ so that it only slightly decreases as α increases. Fig. 5c shows that as β increases, the thermal resistance first decreases and then increases with an optimal value $\beta = 0.72$ for $N = 67$ and $\alpha = 10$, and an optimal value $\beta = 0.84$ for

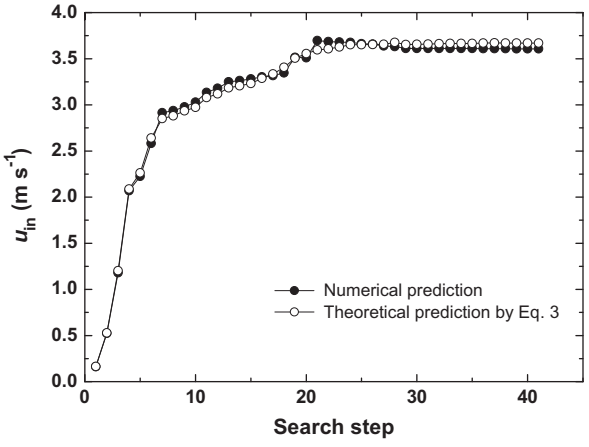

Fig. 6. Validation of inlet flow velocity for fixed pressure drop.

$N = 130$ and $\alpha = 10$. The optimal value of β can be explained by the fact that increasing β not only increases u_{in} and $k_{nf,eff}$ but also increases the conductive thermal resistance and the optimal value of β is determined by competition between these two opposite effect.

5. Optimization at various constraint conditions

Water-based Al_2O_3 nanofluid with 1% particle volume fraction is assumed to be the coolant of the MCHS. The MCHS has $L_x = 10$ mm, $L_y < 1$ mm, $L_z = 10$ mm, and $\delta = 0.1$ mm. The coolant inlet temperature and heat flux are $T_{in} = 293$ K, $q_w = 100$ W cm^{-2}. The constraint conditions are as follows: fixed inlet volume flow rate $Q_V = 200$ cm^3 min^{-1}, fixed pumping power $\Omega = 0.05$ W, and fixed pressure drop $\Delta p = 20$ kPa, respectively.

Generally, the conjugate-gradient-method can search only the local maximum or minimum for objective function J. In order to obtain or at least approach the global optimal design, the same three sets of initial guesses are used for various constraint conditions as follows, initial guess #1: $N = 125$, $\alpha = 12.5$, and $\beta = 0.4$; ini-

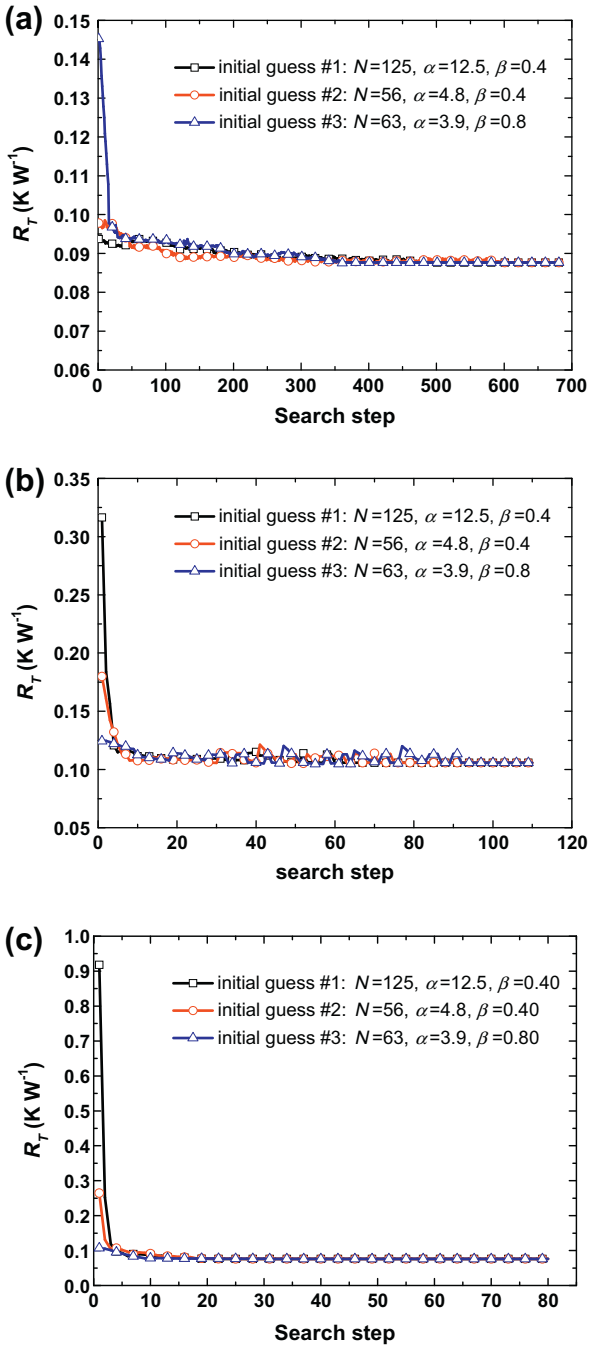

Fig. 7. Variation of total thermal resistance during optimization for various initial guesses: (a) at fixed volume flow rate; (b) at fixed pumping power; and (c) at fixed pressure drop.

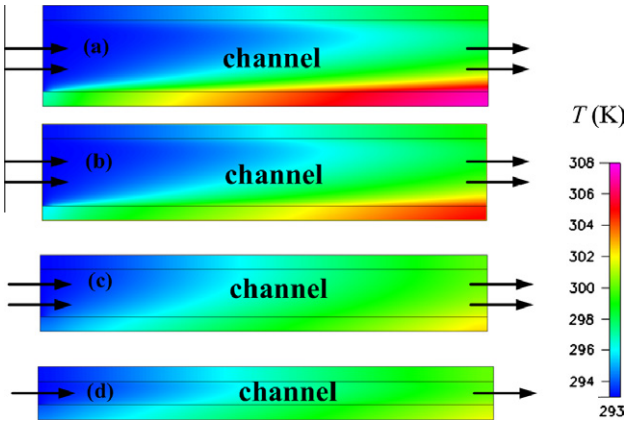

Fig. 8. Temperature distributions in solid and fluid regions along x–y middle cross-section at various search steps for fixed inlet flow volume rate: (a) step 1 (initial guess #3); (b) step 10; (c) step 100; (d) optimal design.

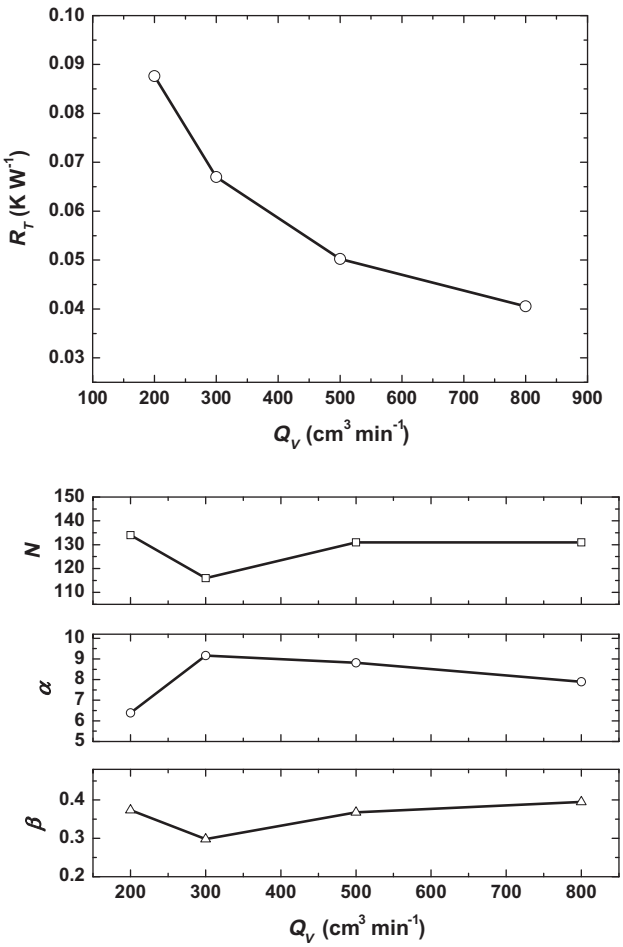

Fig. 9. The effect of inlet volume flow rate on optimal performance of MCHS: (a) thermal resistance; (b) geometric parameters.

tial guess #2: $N = 56$, $\alpha = 4.8$, and $\beta = 0.4$; and initial guess #3: $N = 63$, $\alpha = 3.9$, and $\beta = 0.8$. Fig. 7 shows changes in total thermal resistance, R_T, at each search step for various constraint conditions. The same optimal design is achieved using these initial guesses, which indicates that the obtained optimal design is at least local minimum solution for objective function J. The optimal design has $N = 134$, $\alpha = 6.39$, and $\beta = 0.37$ with thermal resistance of 0.0876 K W^{-1} for fixed volume flow rate of 200 cm^3 min^{-1} (Fig. 7a), $N = 51$, $\alpha = 5.69$, and $\beta = 0.62$ with corresponding thermal resistance of 0.1059 K W^{-1} for fixed pumping power of 0.05 W (Fig. 7b), $N = 37$, $\alpha = 4.38$, and $\beta = 0.59$ with thermal resistance of 0.0760 K W^{-1} for fixed pressure drop of 20 kPa (Fig. 7c).

The temperature distributions in the heat sink at various search steps for the fixed inlet volume flow rate are shown in Fig. 8. For step 1 (initial guess #3) with $N = 63$, $\alpha = 3.9$, and $\beta = 0.8$, the maximum temperature difference in solid and fluid regions is 14.55 K, and it is reduced to 12.11 K for step 10, to 9.42 K for step 100, and to 8.79 K for optimal design. The variation of temperature distributions during optimization for the fixed pumping power and the fixed pressure drop have also similar tendency. The optimal design has larger $N = 134$ as well as smaller $\beta = 0.37$ for fixed inlet volume flow rate, which is in accord with the individual parameter analysis because larger N and smaller β increase the inlet flow velocity and the effective thermal conductivity of nanofluid, and hence enhances convective heat transfer of nanofluid. Different from fixed inlet flow rate, under fixed pumping power and under fixed pressure drop the optimal design has smaller N and larger β, which confirms that selecting the optimal heat sink structure must consider its operation condition.

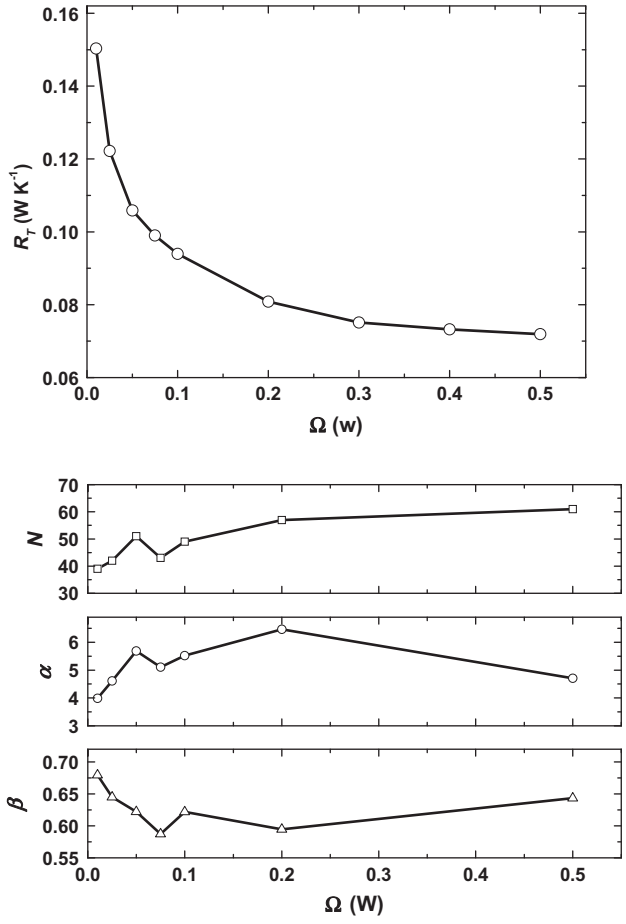

Fig. 10. The effect of pumping power on optimal performance of MCHS: (a) thermal resistance; and (b) geometric parameters.

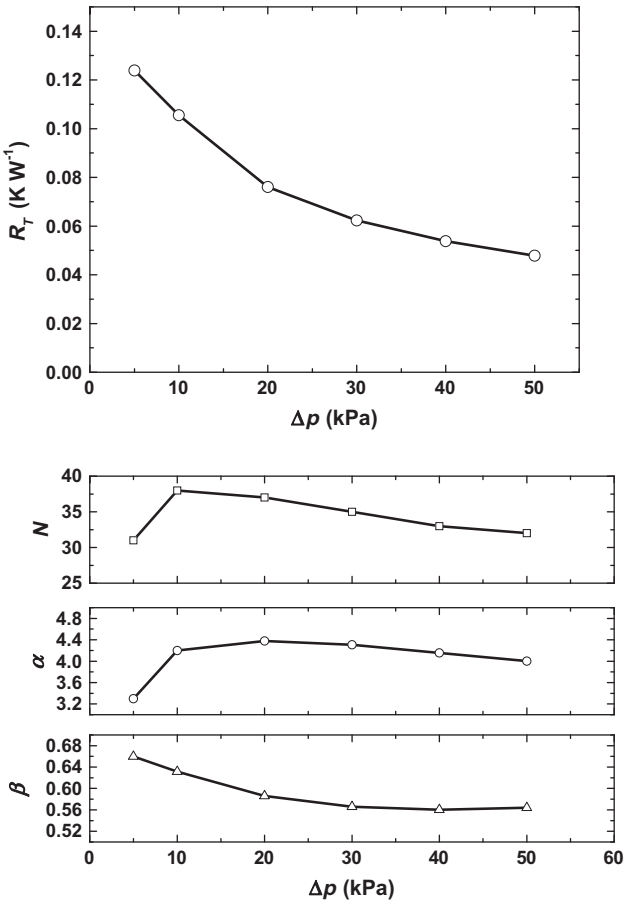

Fig. 11. The effect of pressure drop on optimal performance of MCHS: (a) thermal resistance; and (b) geometric parameters.

The above optimization is complemented at a specific inlet volume flow rate of 200 cm^3 min^{-1}, pumping power of 0.05 W, and pressure drop of 20 kPa, respectively. The optimal geometric structure and corresponding thermal resistance for various volume flow rates, pumping powers, and pressure drops are also calculated using present inverse problem method and are shown in Figs. 9–11. The inlet volume flow rate ranges from 200 cm^3 min^{-1} to 800 cm^3 min^{-1}, with pumping power from 0.01 W to 0.5 W, and pressure drop from 5 kPa to 50 kPa. As the inlet volume flow rate, pumping power, and pressure drop are increased, the thermal resistance is reduced indicating the cooling performance of MCHS is elevated; however, its effectiveness weakens at high flow rate, pumping power, and pressure drop. The optimal range of values for N is 116–134, for α is 6.38–9.16, and for β is 0.30–0.39 under fixed inlet volume flow rates of 200–800 cm^3 min^{-1} (Fig. 9b). However, the optimal range of values for N is 39–61, for α is 3.99–6.47, and for β is 0.59–0.68 under fixed pumping power of 0.01–0.5 W (Fig. 10b), for N is 31–38, for α is 3.29–4.38, and for β is 0.56–0.66 under fixed pressure drop of 5–50 kPa. It is again confirms larger N and smaller β should be adopted when nanofluid-cooled MCHS operates under fixed inlet volume flow rate, however, smaller N and larger β should be adopted when nanofluid-cooled MCHS operates under fixed pumping power or under fixed pressure drop.

6. Conclusions

This work adopted a combined optimization procedure, including a simplified conjugate-gradient method and a completely three-dimensional nanofluid-cooled MCHS model, to look for opti-

mal geometric structure for a silicon-based MCHS. Three parameters, channel number N, channel aspect ratio α, and width ratio of channel to pitch β, server as search variables and are optimized simultaneously under fixed inlet volume flow rate, fixed pumping power, and fixed pressure drop, respectively, with the total thermal resistance R_T as objective function. Water-based Al_2O_3 nanofluid with 1% particle volume fraction is assumed to be the coolant of the MCHS. The MCHS has $L_x = 10$ mm, $L_y < 1$ mm, $L_z = 10$ mm, and $\delta = 0.1$ mm. The coolant inlet temperature and heat flux are $T_{in} = 293$ K, $q_w = 100$ W cm^{-2}.

The optimal geometric structure is closely dependent on the constraint condition. The optimal design has $N = 134$, $\alpha = 6.39$, and $\beta = 0.37$ with thermal resistance of 0.0876 K W^{-1} for fixed volume flow rate of 200 cm^3 min^{-1}, $N = 51$, $\alpha = 5.69$, and $\beta = 0.62$ with corresponding thermal resistance of 0.1059 K W^{-1} for fixed pumping power of 0.05 W, $N = 37$, $\alpha = 4.38$, and $\beta = 0.59$ with thermal resistance of 0.0760 K W^{-1} for fixed pressure drop of 20 kPa.

The optimal geometric structure is different under various inlet volume flow rates, various pumping powers, and various pressure drops. Larger N and smaller β should be adopted when nanofluid-cooled MCHS operates under fixed inlet volume flow rate, however, smaller N and larger β should be adopted when nanofluid-cooled MCHS operates under fixed pumping power or under fixed pressure drop. The improvement in cooling performance of nanofluid-cooled MCHS is attributed that optimal geometric structure increases inlet flow velocity and effective thermal conductivity of nanofluid, which enhances convective heat transfer between nanofluid and channel wall.

Acknowledgments

This study was supported by the National Natural Science Foundation of China (No. 51076009), by National Basic Research Program of China (973 Program, No. 2009CB219803), by the National Natural Science Foundation of China (Nos. 50825603, and U1034004), by Program for New Century Excellent Talents in University (No. NCET-11-0635), and by the Fundamental Research Funds for the Central Universities (No. 11ZG01).

Appendix A

Continuity equation for the nanofluid:

$$\nabla \cdot \vec{V} = 0 \tag{A1}$$

Momentum equation for the nanofluid:

$$\rho_{nf}(\vec{V} \cdot \nabla)\vec{V} = -\nabla p + \mu_{nf}\nabla^2 \vec{V} \tag{A2}$$

Energy equation for the nanofluid:

$$\rho_{nf} c_{p,nf}(\vec{V} \cdot \nabla) T_{nf} = k_{nf,eff}\nabla^2 T_{nf} + \mu_{nf}\left(\frac{\partial V_i}{\partial x_j} + \frac{\partial V_j}{\partial x_i}\right)\frac{\partial V_i}{\partial x_j} \tag{A3}$$

Energy equation for solid region:

$$k_s \nabla^2 T_s = 0 \tag{A4}$$

The boundary conditions are as follows:

$$V = u_{in}, T = T_{in} \quad \text{at } x = 0 \tag{A5}$$

$$\vec{V} = 0, \quad T_s = T_{nf}, \quad k_s \nabla T_s = k_{nf,eff}\nabla T_{nf} \quad \text{at the channel wall-fluid interfaces} \tag{A6}$$

$$q_w = -k_s \frac{\partial T_s}{\partial y} \quad \text{at the bottom wall of heat sink} \tag{A7}$$

$$\nabla T_s = 0 \quad \text{at other outside walls of heat sink} \tag{A8}$$

$$p = p_{out} \quad \text{at } x = L_x \tag{A9}$$

Appendix B

For the sake of convenience, we use $X_1 - X_3$ to denote N, α, and β, respectively, in what follows. The conjugate-gradient method evaluates the gradients of the objective function and sets up a conjugate direction for the updated search variables with the help of a sensitivity analysis. The negative gradient direction of objective function is specified as the first search direction in conjugate gradient method, that is:

$$-\nabla J = \left(-\frac{\partial F}{\partial X_1}, -\frac{\partial F}{\partial X_2}, -\frac{\partial F}{\partial X_3}\right) \tag{A10}$$

where $\partial F/\partial X_i$ is referred to as the sensitivity coefficient. The sensitivity coefficient is calculated by introducing a small perturbation (ΔX_i) to the search variable, X_i. The new search variable, X_i, is updated by:

$$X_i^{(k+1)} = X_i^{(k)} + \beta_i^{(k)}\xi_i^{(k+1)} \quad i = 1,2,3 \tag{A11}$$

where $X_i^{(k)}$ and $X_i^{(k+1)}$ denote values of X_i, in the kth and the $(k+1)$th search steps, respectively; $\beta_i^{(k)}$ denotes the search step size of X_i in the kth search step; $\xi_i^{(k+1)}$ denotes the search direction of X_i, which can be expressed as a linear combination of the previous search direction, $\xi_i^{(k)}$ and the negative gradient direction of new objective function, $-(\partial F/\partial X_i)^{(k+1)}$, that is,

$$\xi_i^{(k+1)} = -\frac{\partial F^{(k+1)}}{\partial X_i} + \gamma_i^{(k+1)}\xi_i^{(k)} \quad i = 1,2,3 \tag{A12}$$

where $\gamma_i^{(k+1)}$ is referred to as the conjugate gradient coefficient, which must guarantee that $\xi_i^{(k)}$ is conjugated to $-(\partial F/\partial X_i)^{(k+1)}$ and expressed as:

$$\gamma_i^{(k+1)} = \left(\frac{\partial F}{\partial X_i}^{(k+1)} \Big/ \frac{\partial F}{\partial X_i}^{(k)}\right)^2 \quad i = 1,2,3 \tag{A13}$$

In basic conjugate-gradient method [25], the optimal search step size, $\beta_i^{(k)}$ ($i = 1, 2, 3$) needs to be determined. After the kth search, the objective function becomes:

$$\begin{aligned} J^{(k)} &= F\left(X_1^{(k)}, X_2^{(k)}, X_3^{(k)}\right) \\ &= F\left(X_1^{(k-1)} + \beta_1^{(k-1)}\xi_1^{(k)}, X_2^{(k-1)} + \beta_2^{(k-1)}\xi_2^{(k)}, X_3^{(k-1)} + \beta_3^{(k-1)}\xi_3^{(k)}\right) \end{aligned} \tag{A14}$$

The value of $\beta_i^{(k)}$ can be acquired by implementing a one-dimensional search with respect to $\beta_i^{(k-1)}$ along the negative gradient direction of the objective function under the condition that other $\beta_j^{(k-1)}$ ($j \neq i$) remain unchanged.

References

[1] Tuckerman DB, Pease RFW. High-performance heat sinking for VLSI. IEEE Electr Dev Lett 1981;2:126–9.
[2] Li J, Peterson GP, Cheng P. Three-dimensional analysis of heat transfer in a micro heat sink with single phase flow. Int J Heat Mass Transf 2004;47:4215–31.
[3] Ryu JH, Choi DH, Kim SJ. Numerical optimization of the thermal performance of a microchannel heat sink. Int J Heat Mass Transf 2002;45:2823–7.
[4] Chen CW, Lee JJ, Kou HS. Optimal thermal design of microchannel heat sinks by the simulated annealing method. Int Commun Heat Mass 2008;35:980–4.
[5] Wang ZH, Wang XD, Yan WM, Duan YY, Lee DJ, Xu JL. Multi-parameters optimization for microchannel heat sink using inverse problem method. Int J Heat Mass Transf 2011;54:2811–9.
[6] Chein R, Huang G. Analysis of microchannel heat sink performance using nanofluids. Appl Therm Eng 2005;25:3104–14.

[7] Koo J, Kleinstreuer C. Laminar nanofluid flow in microheat-sinks. Int J Heat Mass Transf 2005;48:2652–61.
[8] Abbassi H, Aghanajafi C. Evaluation of heat transfer augmentation in a nanofluid-cooled microchannel heat sink. J Fusion Energy 2006;25:187–96.
[9] Jang SP, Choi SUS. Cooling performance of a microchannel heat sink with nanofluids. Appl Therm Eng 2006;26:2457–63.
[10] Tsai TH, Chein R. Performance analysis of nanofluid-cooled microchannel heat sinks. Int J Heat Fluid Flow 2007;28:1013–26.
[11] Li J, Kleinstreuer C. Thermal performance of nanofluid flow in microchannles. Int J Heat Fluid Flow 2008;29:1221–32.
[12] Ghazvini M, Shokouhmand H. Investigation of a nanofluid-cooled microchannel heat sink using fin and porous media approaches. Energ Convers Manage 2009;50:2373–80.
[13] Chen CH, Ding CY. Study on the thermal behavior and cooling performance of a nanofluid-cooled microchannel heat sink. Int J Therm Sci 2011;50:378–84.
[14] Chein R, Chuang J. Experimental microchannel heat sink performance studies using nanofluids. Int J Therm Sci 2007;46:57–66.
[15] Ho CJ, Wei LC, Li ZW. An experimental investigation of forced convection cooling performance of a microchannel heat sink with Al_2O_3/water nanofluid. Appl Therm Eng 2010;30:96–103.
[16] Lelea D. The performance evaluation of Al_2O_3/water nanofluid flow and heat transfer in microchannel heat sink. Int J Heat Mass Transf 2011;54:3891–9.
[17] Wang XQ, Mujumdar AS. Heat transfer characteristics of nanofluids: a review. Int J Therm Sci 2007;46:1–19.
[18] Wen DS, Lin GP, Vafai S, Zhang K. Review of nanofluids for heat transfer applications. Particuology 2009;7:141–50.
[19] Koo J, Kleinstreuer C. A new thermal conductivity model for nanofluids. J Nanopart Res 2004;6:577–88.
[20] Leong KC, Yang C, Murshed SMS. A model for the thermal conductivity of nanofluids – the effect of interfacial layer. J Nanopart Res 2006;8:245–54.
[21] Eapen J, Rusconi R, Piazza R, Yip S. The classical nature of thermal conduction in nanofluids. J Heat Trans – T ASME 2010;132:102402.
[22] Zhao JJ, Duan YY, Wang XD, Wang BX. Effect of nanofluids on thin film evaporation in microchannels. J Nanopart Res 2011;13:5033–47.
[23] Zhao JJ, Duan YY, Wang XD, Wang BX. Effects of superheat and temperature-dependent thermophysical properties on evaporating thin liquid films in microchannels. Int J Heat Mass Transf 2011;54:1259–67.
[24] Nguyen CT, Desgranges F, Roy G, Galanis N, Mare T, Boucher S, et al. Temperature and particle-size dependent viscosity data for water-based nanofluids-Hysteresis phenomenon. Int J Heat Fluid Flow 2007;28:1492–506.
[25] Das SK, Putra N, Thiesen P, Roetzel W. Temperature dependence of thermal conductivity enhancement for nanofluids. J Heat Transfer 2003;125:567–74.
[26] Xuan Y, Roetzel W. Conceptions for heat transfer correlation of nanofluids. Int J Heat Mass Transf 2000;43:3701–7.
[27] Wang XD, Huang YX, Cheng CH, Jang JY, Lee DJ, Yan WM, et al. An inverse geometry design problem for optimization of single serpentine flow field of PEM fuel cell. Int J Hydrogen Energy 2010;35:4247–57.